Electronic Supplementary Material (ESI) for Physical Chemistry Chemical Physics.

UV Laser Photoactivation of Hexachloroplatinate Bound to Individual Nucleobases in Vacuo as Molecular Level Probes of a Model Photopharmaceutical

Edward Matthews, Ananya Sen, Naruo Yoshikawa, Ed Bergström and Caroline E. H. Dessent*

Department of Chemistry, University of York, Heslington, York, YO10 5DD, UK.

*Corresponding Author: Fax: 44-1904-322516. E-mail: caroline.dessent@york.ac.uk

Supplementary Material

S1. Instrumental Details and Experimental Description

UV photons for the laser spectroscopy experiments are provided by an Nd:YAG (Powerlite) pumped OPO (Panther Ex), producing ~2 mJ across the range 215-310 nm. A 200 mm UV fused silica focussing lens is used to reduce the beam diameter to ~2 mm when entering the mass spectrometer and is placed such that the focal point occurs within the mass spectrometer.

The mass spectrometer has been modified as follows for performing the laser experiments (Figure S1). Two laser windows have been installed in the top flange of the vacuum chamber to provide entrance and exit ports for the laser beam. Two 2 mm holes have been drilled through the ring electrodes, thus allowing the laser beam a path through the centre of the trap. The RF circuit was retuned following the drilling of the holes so that the performance of the mass spectrometer is unaffected by these modifications. The Helium pressure within the modified trap is maintained at 5 x 10^{-6} mbar. A pair of mirrors are situated beneath the ion trap to allow the laser beam to exit the mass spectrometer after passing through the ion trap to assists laser alignment.

All instrument parameters and laser experiments are controlled via the AmaZon software. A typical spectral scan sequence consists of: clear ion trap, accumulate ions in trap (typically 20 – 200 ms), mass selected ion isolation within the trap, fragmentation and mass scan. The MS_n functionality of the mass spectrometer is used to store ions for a variable time period (typically 100 – 500 ms) during the fragmentation window in which they are exposed to the laser. The fragmentation stage is commonly used to study the collision induced dissociation of gaseous ions, in a laser scan the CID amplitude is set at 0 V. A beam shutter (Model SH05, Thorlabs Inc) is used to control the laser beam transmission into the mass spectrometer, and is triggered by the mass spectrometer such that the ion trap is only irradiated during the fragmentation phase of the mass spectrum acquisition.

The photodepletion intensity (PD) of the clusters and the photofragment production (PF) have been calculated using equations 1 and 2 and are presented as a function of the photon energy.

$$\text{Photodepletion Intensity} = \frac{\text{Ln}\left(\frac{\text{Int}_{OFF}}{\text{Int}_{ON}}\right)}{\lambda \times P} \qquad [1]$$

$$\text{Photofragmentation Production} = \frac{\left(\frac{\text{Int}_{Frag}}{\text{Int}_{OFF}}\right)}{\lambda \times P} \qquad [2]$$

Where Int_{ON} and Int_{OFF} are the parent peak intensities with laser on and off, Int_{Frag} is the fragment intensity with laser on, λ is the excitation wavelength (nm) and P is the laser pulse energy (mJ). As in the CID experiments, peak intensities are averaged over one minute windows. When isolating the $PtCl_6^{2-}\cdot M$ clusters, small quantities of $PtCl_4^-$ and $PtCl_5^-$ were trapped during the isolation procedure.

These ions (<1% of parent cluster intensity) were minimized by tuning the isolation parameters of the amaZon.

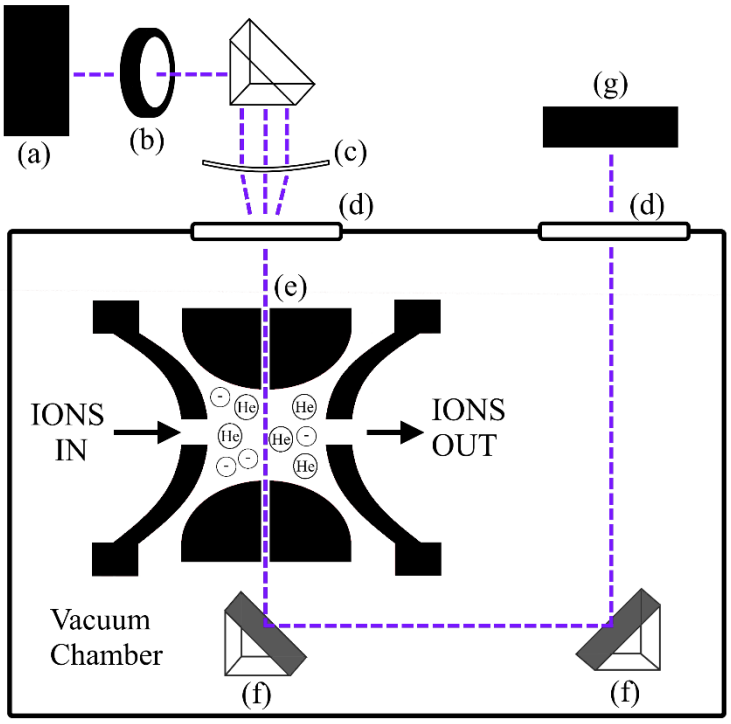

Figure S1: Schematic diagram of the experimental apparatus and the modifications to the Bruker amaZon mass spectrometer that was used to record the photodissociation spectra of the $PtCl_6^{2-}$·M (M = uracil, thymine, cytosine and adenine) clusters. Where (a) is an Nd:YAG (Powerlite) pumped OPO (Panther Ex) tuneable laser source; (b) is an optical shutter (Model SH05, Thorlabs Inc); (c) is a 200 mm focal length UVFS lens (LE4467-UV, Thorlabs Inc); (d) is a pair of flange mounted uncoated UVFS windows (WG41050, Thorlabs Inc); (e) is a 2 mm hole drilled through the ring electrode of the ion trap to allow the passage of laser light; (f) is a pair of mirrors; and (g) is a UV-Vis spectrometer (USB2000+ UV-VIS, Ocean Optics Inc).

S2. TD-DFT calculations of $PtCl_6^{2-}$ and $PtCl_6^{2-}$·M where M = A, C, T

i. TD-DFT calculations of $PtCl_6^{2-}$

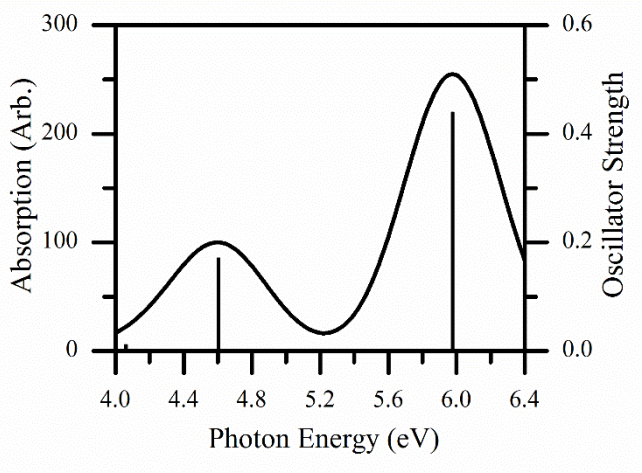

Figure S2: Calculated excitation energies of $PtCl_6^{2-}$ from TDDFT calculations with the M06-2X functional. The oscillator strengths of individual transitions are given by the vertical bars. The full line spectrum represents a convolution of the calculated spectrum with a Gaussian function (0.333 eV HWHM).

Table S1: Calculated transition energies and oscillator strengths of $PtCl_6^{2-}$ from TDDFT calculations with the M06-2X functional.[a,b]

Transition Energy (eV)	Oscillator Strength
$PtCl_6^{2-}$ LMCT Transitions	
4.06	0.0114
4.59	0.1705
5.98	0.4392

[a] Using a split basis set of: 6-311+G(2d,2p) on all first and second row atoms and the Def2-TZVPP basis set to describe the platinum valence orbitals with the 60 core electrons represented by the Stuttgart/Dresden electron core pseudopotential.

[b] All transitions are triply degenerate.

ii. TD-DFT calculations of $PtCl_6^{2-}$·T

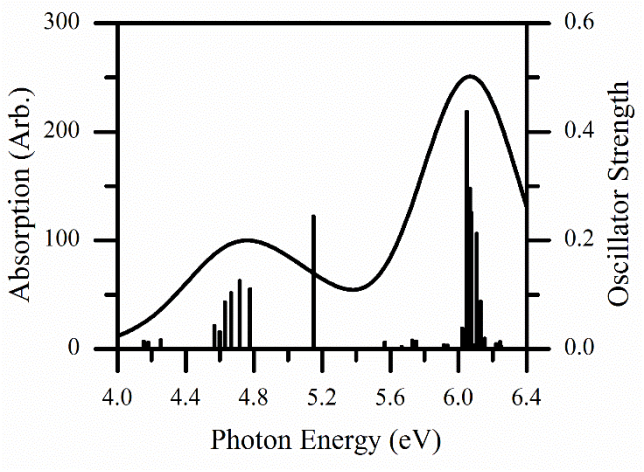

Figure S3: Calculated excitation energies of $PtCl_6^{2-}$·T from TDDFT calculations with the M06-2X functional. The oscillator strengths of individual transitions are given by the vertical bars. The full line spectrum represents a convolution of the calculated spectrum with a Gaussian function (0.333 eV HWHM).

Table S2: Calculated transition energies and oscillator strengths of $PtCl_6^{2-}$·T from TDDFT calculations with the M06-2X functional.[a]

Transition Energy (eV)	Oscillator Strength
$PtCl_6^{2-}$ LMCT Transitions	
4.15	0.0143
4.18	0.0123
4.25	0.0171
4.57	0.0439
4.60	0.0316
4.63	0.0866
4.67	0.1040
4.72	0.1264
4.78	0.1110
5.57[b]	0.0131
Thymine π and $PtCl_6^{2-}$ orbitals→ Thymine π* Transitions[c]	
5.15	0.2449
5.73	0.0167
5.75	0.0145

[a] Using a split basis set of: 6-311+G(2d,2p) on all first and second row atoms and the Def2-TZVPP basis set to describe the platinum valence orbitals with the 60 core electrons represented by the Stuttgart/Dresden electron core pseudopotential.

[b] Transitions originates primarily from a $PtCl_6^{2-}$ orbital with some delocalisation to the thymine.

[c] Thymine π orbitals have a minor delocalisation across the $PtCl_6^{2-}$ moiety.

iii. TD-DFT calculations of $PtCl_6^{2-}$·C

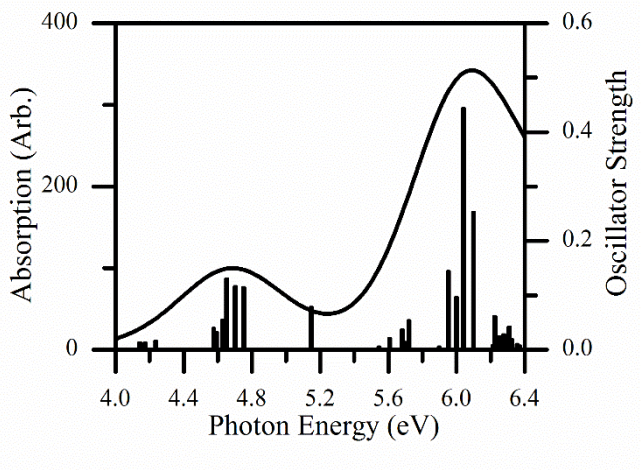

Figure S4: Calculated excitation energies of $PtCl_6^{2-}$·C from TDDFT calculations with the M06-2X functional. The oscillator strengths of individual transitions are given by the vertical bars. The full line spectrum represents a convolution of the calculated spectrum with a Gaussian function (0.333 eV HWHM).

Table S3: Calculated transition energies and oscillator strengths of $PtCl_6^{2-}$·C from TDDFT calculations with the M06-2X functional.[a]

Transition Energy (eV)	Oscillator Strength
$PtCl_6^{2-}$ LMCT Transitions	
4.14	0.0129
4.17	0.0123
4.24	0.0160
4.58	0.0395
4.59	0.0320
4.63	0.0544
4.65	0.1305
4.70	0.1165
4.75	0.1148
5.61[b]	0.0204
5.68[b]	0.0370
5.70[b]	0.0137
Cytosine π and $PtCl_6^{2-}$ orbitals → Cytosine π* Transitions[c]	
5.15	0.0781
5.72	0.0537

[a] Using a split basis set of: 6-311+G(2d,2p) on all first and second row atoms and the Def2-TZVPP basis set to describe the platinum valence orbitals with the 60 core electrons represented by the Stuttgart/Dresden electron core pseudopotential.

[b] A minor contribution to the initial $PtCl_6^{2-}$ orbital by the lone pair of the oxygen on the cytosine.

[c] The initial cytosine orbitals have a minor delocalisation to the $PtCl_6^{2-}$ moiety.

iii. TD-DFT calculations of $PtCl_6^{2-}$·A

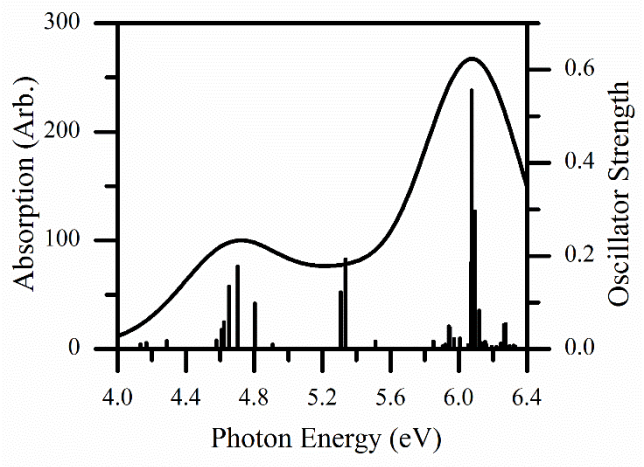

Figure S5: Calculated excitation energies of $PtCl_6^{2-}$·A from TDDFT calculations with the M06-2X and functional. The oscillator strengths of individual transitions are given by the vertical bars. The full line spectrum represents a convolution of the calculated spectrum with a Gaussian function (0.333 eV HWHM).

Table S4: Calculated transition energies and oscillator strengths of $PtCl_6^{2-}$·A from TDDFT calculations with the M06-2X functional.[a]

Transition Energy (eV)	Oscillator Strength
$PtCl_6^{2-}$ LMCT Transitions	
4.61	0.0417
4.62	0.0587
4.65	0.1353
4.70	0.1784
4.80	0.0984
Adenine $\pi \rightarrow$ Adenine Rydberg Transition	
4.91	0.0102
$PtCl_6^{2-}$ and Adenine $\pi \rightarrow$ Adenine π^* Transitions[b]	
5.31	0.1227
5.34	0.1937

[a] Using a split basis set of: 6-311+G(2d,2p) on all first and second row atoms and the Def2-TZVPP basis set to describe the platinum valence orbitals with the 60 core electrons represented by the Stuttgart/Dresden electron core pseudopotential.

[b] $PtCl_6^{2-}$ orbitals show delocalisation to the adenine unit.

S3. Aqueous Absorption Spectra of K_2PCl_6 and the nucleobases U, T, C and A

Solutions of K_2PtCl_6 and the nucleobases were made up in distilled water at a concentration of ~1 x 10^{-5} mol dm^{-3}. UV absorption spectra were recorded using a Shimadzu 1800 UV spectrophotometer with a 1 cm UV cuvette, using distilled water as a baseline. The aqueous absorption spectra were converted to molar absorption coefficients using the Beer-Lambert law. Graphs of excitation energy against molar absorption coefficient for the five aqueous molecules are given in Figure S6. The photon energies which gave the maximum absorption (λ_{max}) and the corresponding molar absorption coefficients (ε_{max}) are summarised in Table S5. Table S5 shows that the maximum absorption of each of the molecules studies occurs between 4.6 – 4.8 eV in distilled water. Aqueous $PtCl_6^{2-}$ has a stronger chromophore than the nucleobases by approximately 2x for adenine, 3x for uracil and thymine, and 8x for cytosine.

Table S5: Aqueous absorption maxima and molar absorption coefficients of K_2PtCl_6 and the nucleobases uracil, thymine, cytosine and adenine.

Molecule	λ_{max} / eV	ε_{max} / dm^3 mol^{-1} cm^{-1}
Uracil	4.79	6080
Thymine	4.69	6440
Cytosine	4.63	2180
Adenine	4.76	8520
K_2PtCl_6	4.73	18300

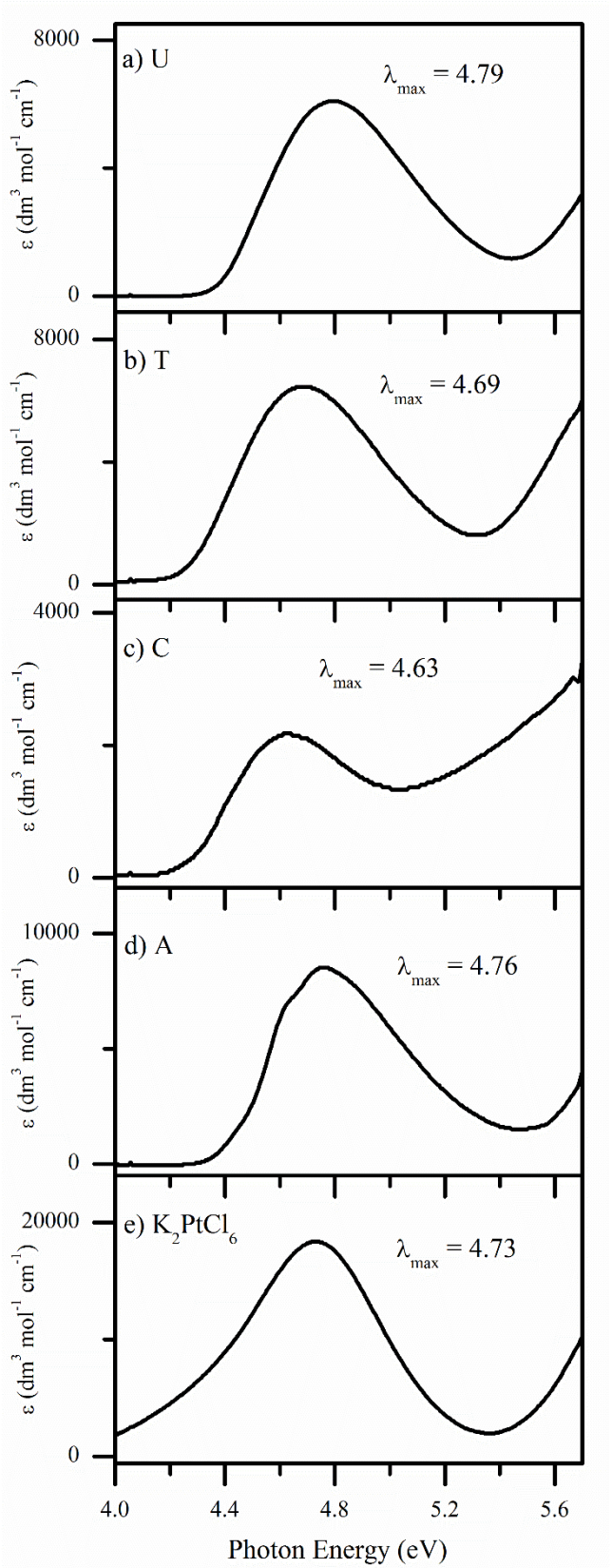

Figure S6: Aqueous molar absorption coefficients of: a) Uracil, b) Thymine, c) Cytosine, d) Adenine and e) K_2PtCl_6 across the range 4.0 – 5.7 eV.

S4. Additional Photofragment Mass Spectra and Action Spectra for $PtCl_6^{2-}$·M, M = U, T, C, A

a) Electron detached fragments of $PtCl_6^{2-}$·A

A series of low intensity fragments are observed in the high mass region of the $PtCl_6^{2-}$·A photofragment mass spectra, Figure S7, consistent with deprotonated adenine coordinating to the platinum via the loss of HCl. These fragments are only seen as singly negatively charged species, suggesting that these reactions are only possible following electron detachment. This behaviour is unique to adenine amongst the studied nucleobases. Chemical formulae were assigned by comparing the recorded fragmentation patterns with patterns simulated using the Compass DataAnalysis (Bruker) software package (An example is given in Figure S8).

Collision induced dissociation (CID) was performed on the $PtCl_6^-$·A and $[PtCl_5(A\text{-}H)]^-$ fragments, Figures S9 and S10, by utilising the MS3 capabilities of the mass spectrometer. The CID spectra show that $PtCl_6^-$·A thermally decays into $PtCl_6^-$ and $[PtCl_5(A\text{-}H)]^-$ with a high conversion efficiency, $PtCl_4^-$ is produced as a minor fragment. $[PtCl_5(A\text{-}H)]^-$ thermally dissociates into two lower mass $[PtCl_x(A\text{-}nH)]^-$ fragments as well as $PtCl_4^-$ and $PtCl_5^-$. Figures S9 and S10 shows that there is a thermal production route for the high mass fragments of $PtCl_6^{2-}$·A that are seen in Figure S7; $PtCl_6^-$·A is a primary electron detached fragments, the other high mass fragments are assigned as secondary electron detached fragments.

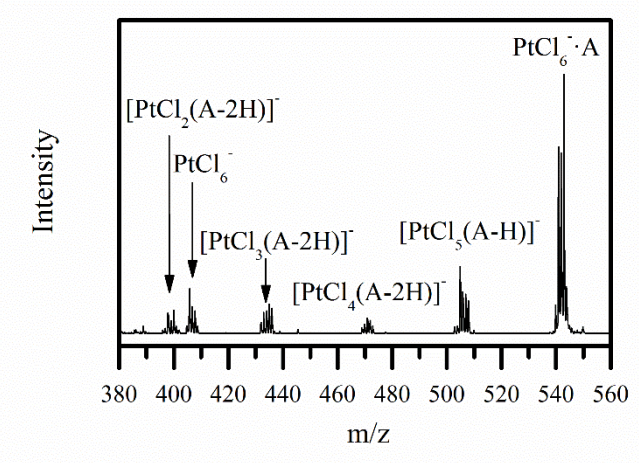

Figure S7: Photofragment mass spectrum of $PtCl_6^{2-}$·A irradiated at 280 nm, highlighting the electron detached fragments within the high mass region of the spectrum.

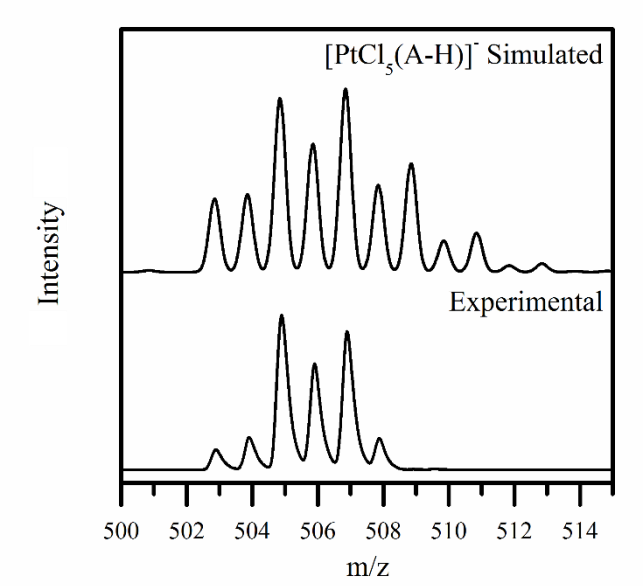

Figure S8: A comparison between a simulated isotope pattern of $[PtCl_5(A\text{-}H)]^-$ with the corresponding mass spectrum of $PtCl_6^{2-}\cdot A$ irradiated at 280 nm. The simulated patterns were generated using the Compass DataAnalysis (Bruker) software package.

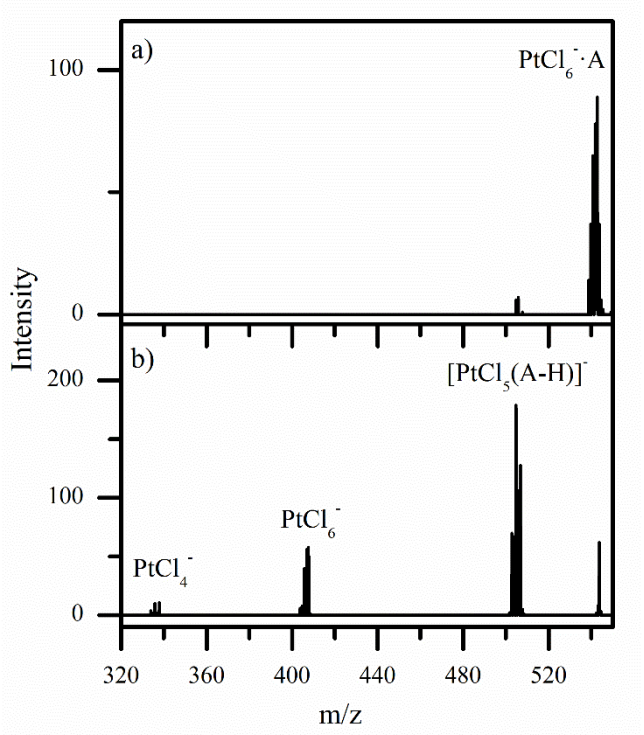

Figure S9: Collision induced dissociation mass spectrum of the $PtCl_6^-\cdot A$ fragment with an excitation voltage of a) 0 V and b) 0.2 V. $PtCl_6^-\cdot A$ was isolated and fragmented, following its photoproduction with an excitation wavelength of 260 nm, using the MS3 capabilities of the mass spectrometer

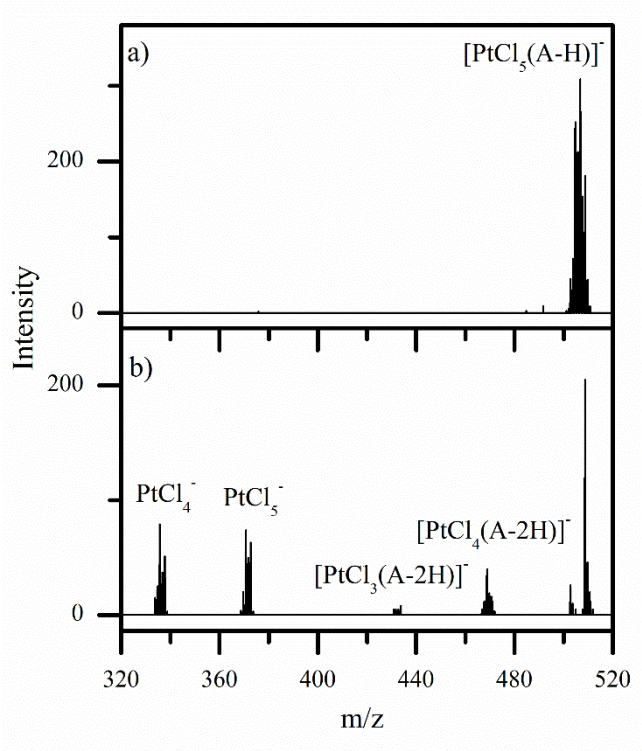

Figure S10: Collision induced dissociation mass spectrum of the $[PtCl_5(A\text{-}H)]^-$ fragment with an excitation voltage of a) 0 V and b) 0.4 V. $[PtCl_5(A\text{-}H)]^-$ was isolated and fragmented, following its photoproduction with an excitation wavelength of 260 nm, using the MS3 capabilities of the mass spectrometer

b) Photofragment Mass Spectra at 215 nm

The photofragment mass spectrum with an excitation wavelength of 215 nm (5.77 eV) is provided, Figure S11, to highlight the differences and similarities between the photofragment mass spectrum at 4.77 eV (Figure 5). It can be seen that electron detachment is a far more prominent fragmentation channel at 215 nm; production of $PtCl_x^-$ (x=3-5) is comparable between the two wavelengths; $PtCl_6^{2-}$ is quenched at 215 nm; and $[M\text{-}H]^-$ is more significant, relative to $M\cdot Cl^-$, at 215nm.

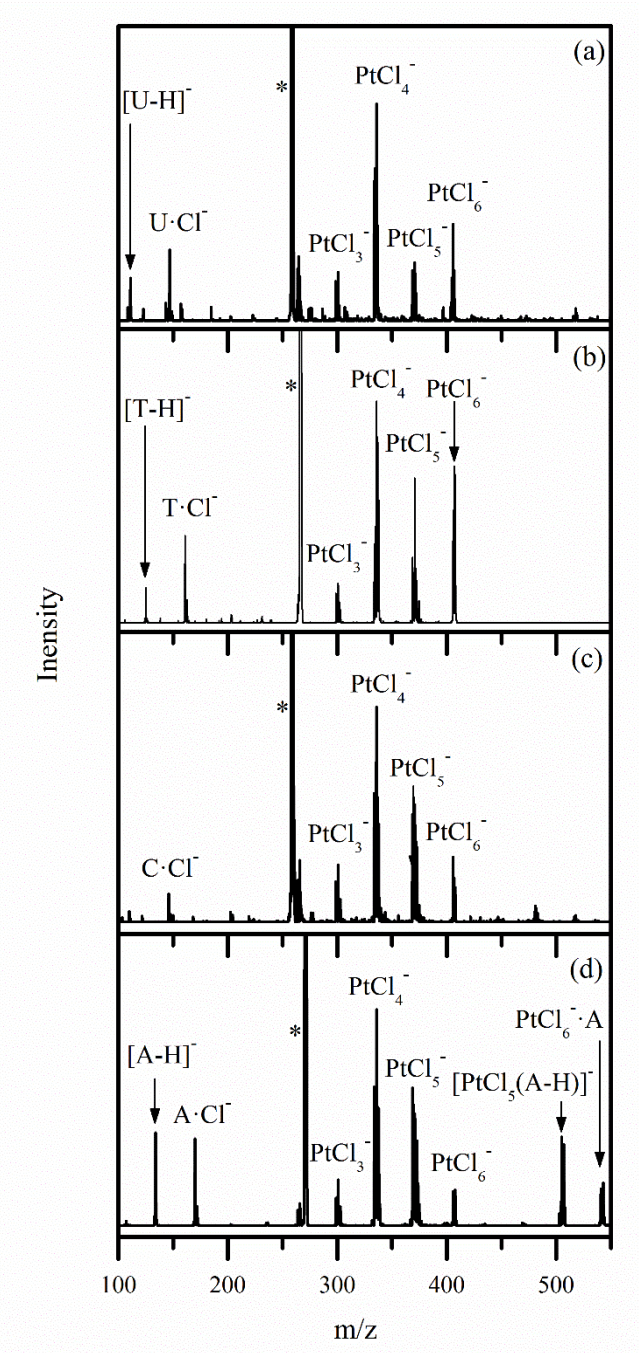

Figure S11: Photofragmentation mass spectra (laser on) of the $PtCl_6^{2-}$·M clusters obtained at 5.77 eV (215 nm) where M = (a) uracil, (b) thymine, (c) cytosine, (d) adenine. The parent peak is denoted by the *.

c) Photoproduction Spectra of $PtCl_4^-$ and $PtCl_3^-$

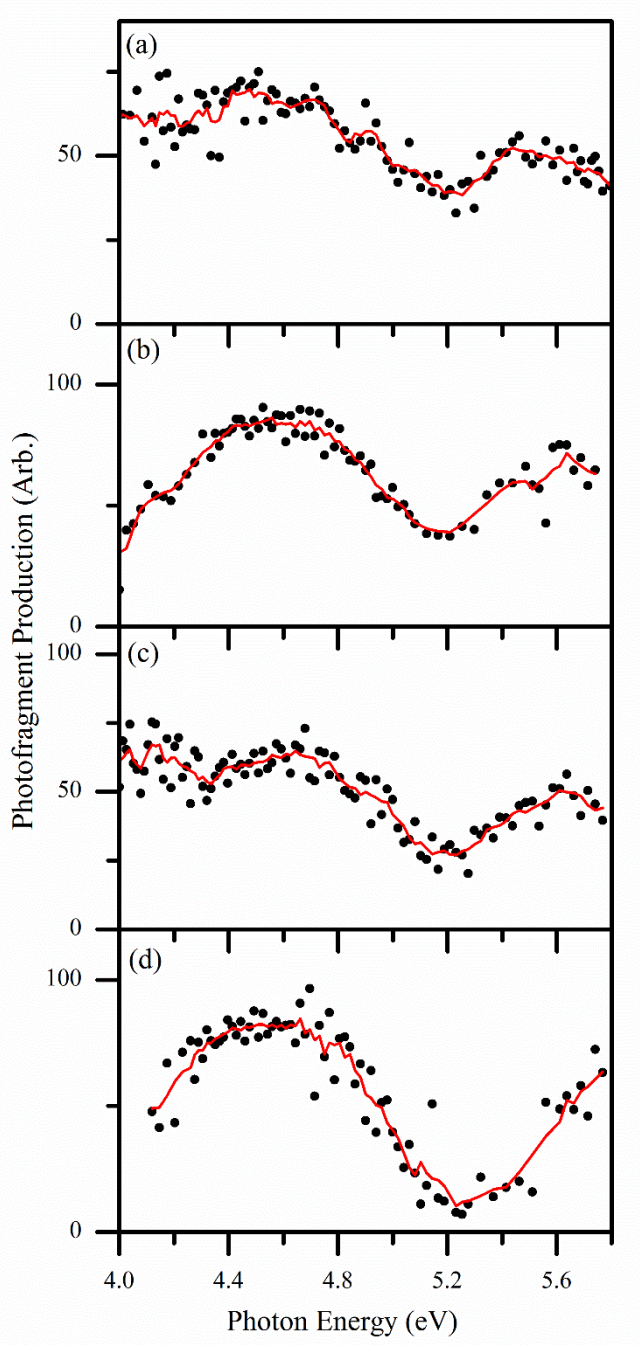

Figure S12: Photofragment production spectra of the $PtCl_4^-$ photofragment produced from (a) $PtCl_6^{2-}$·U, (b) $PtCl_6^{2-}$·T, (c) $PtCl_6^{2-}$·C and (d) $PtCl_6^{2-}$·A. The $PtCl_4^-$ photoproduction intensities are corrected for trapping impurities by subtracting the intensity of $PtCl_4^-$ recorded in the corresponding scan without laser.

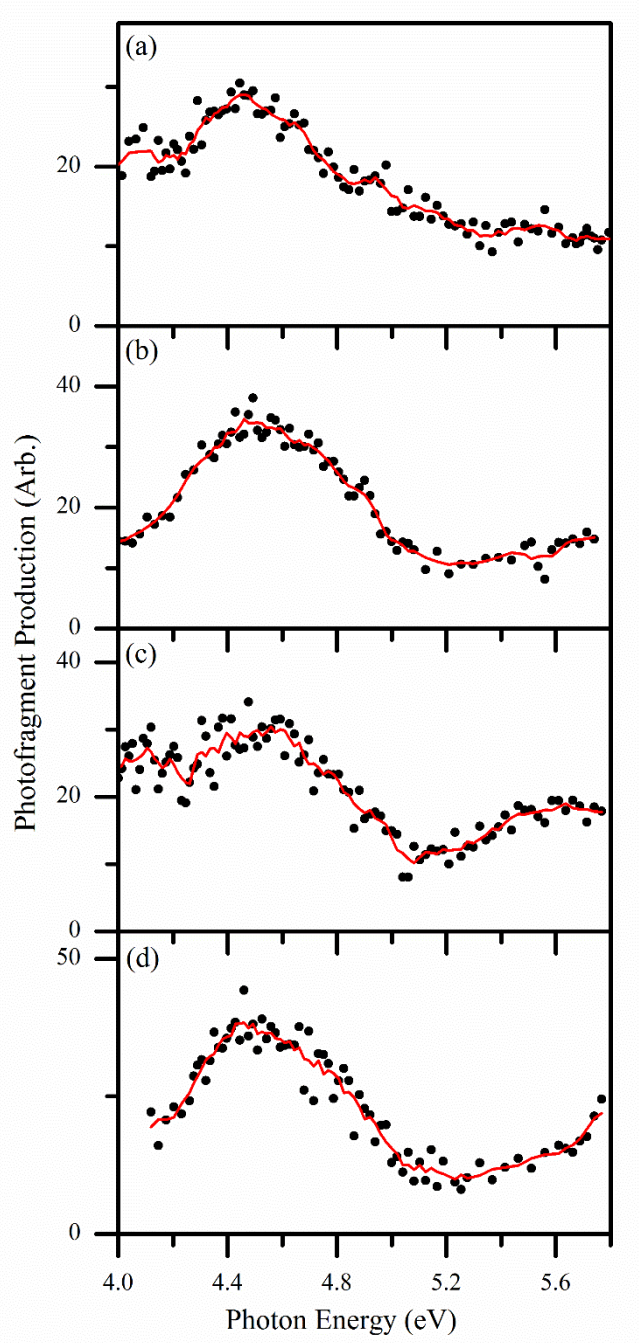

Figure S13: Photofragment production spectra of the $PtCl_3^-$ photofragment produced from a) $PtCl_6^{2-}$·U, b) $PtCl_6^{2-}$·T, c) $PtCl_6^{2-}$·C and d) $PtCl_6^{2-}$·A. These spectra generally match the trends of the $PtCl_4^-$ spectra.

S5. Energetics of Fragmentation Pathways for the $PtCl_6^{2-}$·A Cluster.

Six fragmentation pathways were selected to describe the production of charged fragments following electronic excitation of the $PtCl_6^{2-}$·A cluster. The reaction energies were calculated by comparing the difference in the computed SCF energies between products and reactants. All structures and energies were calculated using Gaussian 09 employing the M06-2X functional with the basis sets and electron-core pseudopotential described in Section 2 of the main text. Frequency calculations were performed on the optimised structures to show that they are minima.

Table S6: Calculated photofragmentation reaction energies from the $PtCl_6^{2-}$·A cluster, calculated using Gaussian 09 using the M06-2X functional. Production energies show the total energy change to produce the photofragments from $PtCl_6^{2-}$·A.[a]

Reaction	Parent	Fragments	Reaction Energy (eV)	Production Energy[a] (eV)
1	$PtCl_6^{2-}$·A	$PtCl_6^{2-}$ + A	1.35	-
2	$PtCl_6^{2-}$·A	$PtCl_5^-$ + A·Cl^-	-0.551	-
3	$PtCl_6^{2-}$	$PtCl_5^-$ + Cl^-	-0.726	0.622
4	A·Cl^-	$[A\text{-}H]^-$ + HCl	1.57	1.01
5	$PtCl_5^-$	$PtCl_4^-$ + $Cl^\cdot$	1.72	1.16 (2.73)[b]
6	$PtCl_4^-$	$PtCl_3^-$ + $Cl^\cdot$	2.40	3.56 (5.13)[b]

[a] Production energies represent the sum of the constituent reactions to produce this set of photofragments.

[b] Selected reaction energies also include the production of $[A\text{-}H]^-$ and HCl via reaction 4.